On Efficient Non-Stationary Channel Emulation in Conductive Phase Matrix Setup for Massive MIMO Performance Testing

Wang, Heng; Wang, Weiming; Wu, Yongle; Zhang, Guojin; Tang, Bihua; Liu, Yuanan; Pedersen, Gert Frølund; Fan, Wei

Published in:
I E E E Transactions on Vehicular Technology

DOI (link to publication from Publisher):
10.1109/TVT.2022.3175906

Publication date:
2022

Document Version
Accepted author manuscript, peer reviewed version

On Efficient Non-Stationary Channel Emulation in Conductive Phase Matrix Setup for Massive MIMO Performance Testing

Heng Wang, Weimin Wang, *Senior Member, IEEE,* Yongle Wu, *Senior Member, IEEE,* Guojin Zhang, Bihua Tang, Yuanan Liu, *Member, IEEE*, Gert Frølund Pedersen, *Senior Member, IEEE* and Wei Fan, *Senior Member, IEEE,*

***Abstract*—Massive multiple-input multiple-output (MIMO) is considered as a critical technique in 5G New Radio (NR), due to its capability to significantly improve data rate and link reliability for the radio link. To make it a reality, it is essential to evaluate massive MIMO performance in realistic spatial fading channel conditions. Specifically, dynamic spatial channel emulation is crucial to evaluate the massive MIMO beam operations. Due to the high cost associated with both the traditional conduced testing method and the standardized multi-probe anechoic chamber (MPAC) based Over-the-Air (OTA) testing setup for massive MIMO performance testing, fading channel emulation for massive MIMO testing using a conductive phase matrix setup has been proposed in the literature. However, it is still a challenging problem to emulate dynamic spatial channels in a cost-effective and efficient manner for the conductive phase matrix setup, since traditional algorithms suffer from high computational complexity and system cost. This paper proposes a fast and accurate framework to emulate dynamic spatial channels in the phase matrix setup, where the basic idea is to mimic a virtual MPAC setup. By doing so, we can mimic MPAC setup with flexible probe configurations. Furthermore, a novel successive cancellation strategy and a closed-form algorithm are proposed to determine the probe locations and probe weights, respectively, which can significantly reduce the computational complexity associated with dynamic channel emulation. Simulation results show that the proposed algorithm is highly accurate and computationally efficient, compared to state-of-art solutions. Further, we apply our developed algorithm to emulate measured non-stationary channels and excellent emulation accuracy can be achieved. The proposed method can be employed for emulating dynamic spatial channels, which is of great importance for massive MIMO performance testing.**

***Index Terms*—Channel emulation, massive MIMO, phase matrix, virtual over-the-air testing, virtual probe.**

This work was supported by The Key-Area Research and Development Program of Guangdong Province, China (2019B010157001). The BUPT Excellent Ph.D. Students Foundation (No. CX2021216). The National Natural Science Foundations of China (No. 61821001). *(Corresponding author: Weimin Wang.)*

Heng Wang is with the Beijing Key Laboratory of Work Safety Intelligent Monitoring, Department of Electronic Engineering, Beijing University of Posts and Telecommunications, Beijing 100876, China, and also with the Antenna Propagation and Millimeter-wave Systems (APMS) Section, Department of Electronic Systems, Faculty of Engineering and Science, Aalborg University, 9220 Aalborg, Denmark. E-mail: hengwang@bupt.edu.cn.

Weimin Wang, Yongle Wu, Bihua Tang, and Yuanan Liu are with the Beijing Key Laboratory of Work Safety Intelligent Monitoring, Department of Electronic Engineering, Beijing University of Posts and Telecommunications, 100876 Beijing, China. E-mail: wangwm@bupt.edu.cn, wuyongle138@gmail.com, bhtang@bupt.edu.cn, and yuliu@bupt.edu.cn.

Guojin Zhang, Gert Frølund Pedersen and Wei Fan are with the Antenna Propagation and Millimeter-wave Systems (APMS) Section, Department of Electronic Systems, Faculty of Engineering and Science, Aalborg University, 9220 Aalborg, Denmark. E-mail: guojin@es.aau.dk; gfp@es.aau.dk; wfa@es.aau.dk.

I. Introduction

MASSIVE multiple-input multiple-output (MIMO) composed of a large number of antenna elements is utilized for dealing with the stringent communication requirement of 5G [1][2]. By forming narrow beams in the target spatial directions and keeping deep nulls in the interference directions, a massive MIMO device is capable of serving simultaneously multiple terminals in the same time-frequency resources, which boosts the spectral efficiency [3]. To make the massive MIMO systems a reality, performance evaluation is an essential step in product design and refinement. The massive MIMO systems, however, have posed unprecedented challenges on the performance testing methods. In the actual massive MIMO system, the beam operations such as beam allocation, alignment, and tracking would occur typically in highly dynamic scenarios [4]. Thus to evaluate the performance of massive MIMO-type base station (BS), it is essential to emulate a realistic and dynamic multi-dimensional fading channel, which is different from the conventional user equipment (UE) testing where stationary channels are generally assumed [5].

Roughly speaking, Over-the-Air (OTA) method and conductive method are two main methodologies to evaluate the wireless device performance. Multi-probe anechoic chamber (MPAC) [6][7] has been developed for many years for the performance testing of the fourth generation (4G) UE, and it was already standardized [8] and in commercial use for the traditional 4G LTE MIMO handsets. Compared with the uncontrollable field trials in open propagation environment, it is capable of enabling the performance evaluation for the device under test (DUT) in repeatable and controllable laboratory conditions. In addition, extensive efforts have been done for the OTA testing of the fifth generation (5G) New Radio (NR) MIMO handsets in the 3GPP [9]. MPAC is selected as the reference test methodology for the performance verification of 5G NR mobile terminal, where 2D MPAC composed of 16 uniformly distributed dual-polarized probes is adopted for the 5G frequency range (FR)1 handsets [10] and 3D MPAC composed of 6 non-uniformly distributed dual-polarized probes is adopted for the 5G FR2 handsets [10]. However, it is problematic for the massive MIMO BS testing

with MPAC methodology. The large array aperture with high spatial resolution requires a larger number of probe antennas and the associated channel emulator (CE) resources [11]. On the other hand, the large electrical size of massive MIMO BS requires a large facility to meet the far-field measurement criterion [12]. Thus, the existing MPAC based OTA setups for the traditional MIMO handsets suffer from the cost-prohibitive problem for the massive MIMO BS testing. Furthermore, dynamic channel emulation in the MPAC setup, though highly important, is not well discussed in the literature. In one recent publication [13], computational complexity is identified as one of the key technical challenges for dynamic channel emulation in physical MPAC setup.

For the FR1 massive MIMO devices which typically provide the antenna radio frequency (RF) connectors, the traditional conductive testing setup can be employed. However, though widely utilized for testing mobile terminals, the conductive setup, which requires one RF cable connection between each CE interface port and DUT antenna port, is not suitable for massive MIMO-type radio performance testing, due to the fact that the CE resource might become too demanding [14], as a result of a large number of antenna ports in the massive MIMO system.

To tackle the above dilemma, a phase matrix composed of phase shifters and combining units is introduced between the DUT and the CE [15]. It is a conductive method for FR1 massive MIMO testing. As discussed in [15], the phase response among the array elements in the massive MIMO DUT can be emulated using the phase matrix network for any spatial path, and naturally, multi-path fading can be emulated for the DUT. This method is cost-effective and is considered a highly promising methodology in the industry [15][16]. However, the method to determine the optimal virtual path directions and path power weights has not been addressed in the literatures for dynamic channel emulation. To this end, the contributions of this paper are listed below:

- A virtual OTA framework implemented with the phase matrix is proposed where the key research question is how to obtain the optimal path direction and power weight for each virtual path, so as to accurately reconstruct the target channel characteristics with limited system resources. An efficient algorithm based on the successive cancellation (SC) principle is proposed to obtain the optimal virtual probe (path) locations. Compared to traditional works, the optimal probe placement can be obtained directly, with excellent accuracy achieved.
- A simple closed-form probe (path) weighting strategy is derived, to avoid time-consuming numerical optimization procedure. The proposed SC principle and closed-form weighting structure are key to meet the requirement of dynamic channel emulation for practical systems.

In this work, we aim to emulate the dynamic channel at each time snapshot. Its extension to multiple channel snapshots is straightforward by simply repeating the procedure or employing interpolation techniques [17][18], and thus not addressed in this work. Therefore, this paper focuses on the channel emulation with conductive phase matrix setup for a single snapshot, and the implementation of interpolation was detailed in [17]. In addition, the proposed methods can be applied to the channel emulation for not only massive MIMO BS channels, but also the other dynamic scenarios, such as the novel geometry-based MIMO channel for the unmanned aerial vehicle networks proposed in [19], the non-stationary channel for the vehicle communication [20], and so on [21-23].

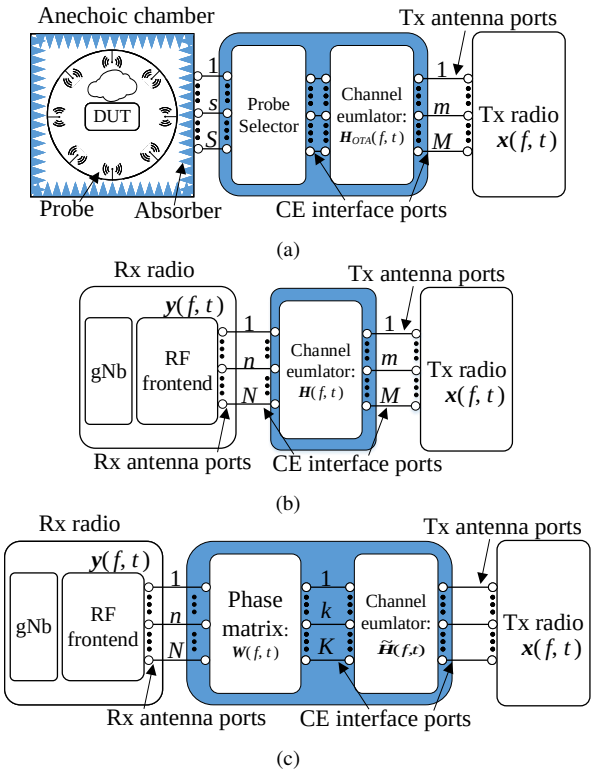

Fig. 1. The illustrations of three testing systems: (a) MPAC setup, (b) traditional conductive testing setup, (c) conductive phase matrix setup.

This paper is organized as follows. In Section II, we outline the principles, pros, and cons of the three existing methodologies. In Section III, we discuss the signal model of the conductive phase matrix setup and channel emulation. In Section IV, we discuss the state-of-art solution for the conductive phase matrix setup and the proposed algorithm. In Section V, the performance of the proposed method is evaluated with 3GPP standard channel models, as well as the real measured dynamic channel in a practical classroom scenario. Conclusion follows in Section VI.

II. Problem Statement

In this section, the MPAC setup and the traditional conductive testing setup are briefly revisited, and the problems of the existing solutions are also discussed. Then we introduce the principle of the conductive phase matrix method. Fig. 1 shows the diagrams of these three methodologies. M is the number of interface ports used to connect the CE at the UE side. For the communication with a terminal equipped with 2 antennas, $M = 2$ CE interface ports are required. Furthermore, for the testing of multi-user communication or adaptive beamforming terminals equipped with more antennas [24], more CE interfaces are needed to connect to the UE

side, aggravating the shortage of CE resources. N is the number of the antenna ports in a massive MIMO array. As illustrated in [25][26], the sub-6 GHz massive MIMO arrays are generally equipped with dozens to hundreds of antenna elements. $x(f,t) \in \mathbb{C}^{1\times N}$ and $y(f,t) \in \mathbb{C}^{M\times 1}$ are the transmitted and the received signal vector, respectively.

A. MPAC Setup

In conventional MPAC setup, multiple probe antennas are uniformly placed in an anechoic chamber to emulate the multi-path environment, with the help of the CE. Fig. 1(a) illustrates the downlink (i.e. communication link from BS to terminal) MPAC setup, S is the number of active probes in MPAC methodology. Considering the tradeoff between emulation accuracy and hardware costs, the number S of active probes is generally limited to no more than 16. $\boldsymbol{H}_{OTA}(f,t) \in \mathbb{C}^{S\times M}$ is the channel impulse response (CIR) matrix, containing the target temporal characteristic, frequency characteristic, Cross Polarization Ratio (XPR) and so on, generated in CE for the S probes [6]. Thus, the objective of the channel emulation algorithm is to reproduce the spatial channels within the test zone by setting proper CIRs in the CE, according to the target channel model and the probe configuration. Mainly two methodologies, i.e. plane wave synthesis (PWS) technique and prefaded signal synthesis (PFS) technique, have been proposed for channel emulation. Note that the hardware platform is the same both for the PWS and the PFS methods.

Using the PWS technique, static plane wave from an arbitrary impinging direction can be synthesized within the test area by appropriately setting complex weights for probes [27][28]. With PWS each plane wave with a specific impinging angle can be generated within the test zone [29], and the spatial characteristics of the target channel can therefore be emulated. One of the limitations of the PWS technique lies in its phase calibration. As discussed in [11], the PWS technique requires accurate phase coherent control for synthesizing the target channel, and the phase and amplitude calibration is therefore required. On the other hand, for the large size device, more probes are required to create a large test area [6]. Specifically, it has been concluded in [11] that with the PWS technique hundreds of probe antennas and associated CE resources would be needed to emulate the spatial channel models for massive MIMO-type DUTs, leading to cost-prohibitive setups. Compared with the PWS method, where the target channel is reconstructed subpath-wise, the PFS technique aims to reconstruct the target channel based on spatial clusters. As illustrated in [6], clusters are mapped to the probes in MPAC, based on the cluster power angular spectrum (PAS) and the probe directions. Thus the multi-cluster environment can be reconstructed by properly allocating power weights for probes. Compared to the PWS method, the number of active probes with PFS is much less [11] for massive MIMO-type DUT. In addition, phase control is not required for PFS, and only amplitude calibration should be performed. One of the disadvantages of PFS is that it can not reproduce the line-of-sight (LOS) (specular) path with the direction where probes are not located [29]. On the other hand, the emulation accuracy for clusters with small angle spread depends on the probe spacing. The smaller the cluster angle spread, the smaller the probe spacing is required for the PFS method. Thus compared with the PWS method, although the required CE resources are saved, a densely distributed probe panel is needed as well for the 3D massive MIMO BS channel emulation [11]. Furthermore, take an 8×8 planar array ($N = 64$) with 0.5 wavelength spacing operating at 2.6GHz as an example, the aperture is about 0.58m, requiring more than the measurement distance of 5.8m to meet the Fraunhofer far-field criterion in MPAC.

The probe selection strategy, inspired by the fact that radio channels are often directive and not all probe antennas contribute equally in the channel emulation, is proposed to reduce the system cost. However, it is still not widely adopted in the industry, due to the practical difficulties of implementing the probe selection framework, e.g. massive switching circuits [29]. Furthermore, the computational complexity of existing probe selection algorithms is incompetent for dynamic channel emulation. Specifically, there are generally two types of probe selection algorithms: the iterative algorithms [30][31], and the heuristic algorithms [32][33]. All of them are too time-consuming, due to their inherent selection principle which requires redundantly calculating the contributions of all the available probe directions. Although a simple algorithm, referred to as the spatial angle mapping (SAM) algorithm, was proposed [11] and was applied to emulate the dynamic channel [13], the emulation accuracy is relatively insufficient due to the fact that some weak clusters may be ignored [11]. Furthermore, for dynamic channels, we need to be able to emulate channels at snapshot level [34], not only at the cluster level. SAM algorithm, however, only works for cluster-based channel models.

B. Traditional Conductive Setup

Regarding the full conductive test methodology, CE provides the full $N \times M$ MIMO fading channel $H(f,t) \in \mathbb{C}^{N\times M}$ which is the propagation channel matrix in real world. Fig. 1(b) shows the framework of the traditional full conductive setup, where N antenna ports at receiver (Rx) side are connected to the CE interface ports which are then connected to M antennas at transmitter (Tx) side, via coaxial cables. For the traditional conductive setup, we need N+M physical interface ports in the CE and M·N logical channels for a uni-directional (i.e. either downlink or uplink) transmission. Obviously, the need for fading emulator resources is directly proportional to the number of antennas, N and M. For instance, using this setup, the testing of a massive MIMO array containing 256 antenna ports would require more than 256 CE interface ports, which is not practical due to cost consideration.

C. Conductive Phase Matrix Setup

A conductive phase matrix setup together with the CE is introduced to reduce the amount of required fading emulation resources, as shown in Fig. 1(c). There are one-to-many phase-adjustable connections in the phase matrix between each input port and the N output ports, which is capable of adjusting the

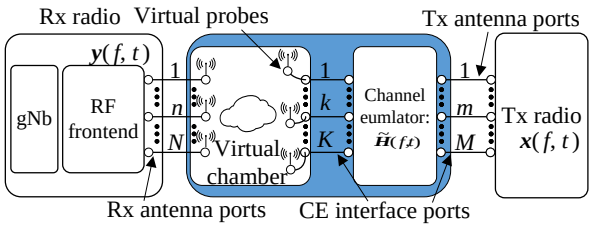

Fig. 2. The virtual MPAC setup which is the equivalent diagram of conductive phase matrix setup.

phase of the connections between each input port and each output port, to emulate the expected array response modeled by the predefined spatial direction, as if there exists an OTA probe in an anechoic chamber. Since the array responses are generated by phase matrix, rather than the real propagation, the probe (path) is referred to as the virtual probe in the paper. K is the number of virtual probes in our proposed solution. The employed number K of virtual probes is no more than 16 as well in our research. $\widetilde{\boldsymbol{H}}(f,t) \in \mathbb{C}^{K\times M}$ is a channel matrix including $K \cdot M$ cross-channels generated in CE which could satisfactorily provide the effects of temporal and frequency fading, antenna characteristics, the noise interferences, and the user side effects.

Thus the main difference between $\widetilde{\boldsymbol{H}}(f,t)$ and $\boldsymbol{H}_{OTA}(f,t)$ is that the $\boldsymbol{H}_{OTA}(f,t)$ is for the real probes with fixed locations, while $\widetilde{\boldsymbol{H}}(f,t)$ is for the virtual probes with arbitrary locations. Fig. 2 shows the equivalent diagram, which follows analogy with the MPAC setup, but this method will not suffer from the limitations of probe spacing, probe panel coverage, and DUT mechanical rotation in MPAC. On the other hand, the phase matrix could easily realize not only the function of probe switching but also the far-field array responses [35], which is important for beamforming testing [15]. Compared to the conventional conductive setup, the number of the required physical CE ports can be reduced from N to K, using the conductive phase matrix setup. Consequently, the key question is how to emulate dynamic channels with minimum K in a cost-effective and computationally efficient manner. In the following section, the channel emulation in the spatial domain is detailed. Particularly, the channel characteristic realizations in other domains are implemented in CE, and then connected to the phase matrix. Note that before practical application, amplitude and phase calibration is required for the phase matrix to normalize the response differences between each input and output RF chain [15]. In addition, it was concluded in [15] that, even if the phase matrix is discretely controlled, the channel emulation performance is very close to that with continuous phase control. And this conclusion holds for a large number of array elements as well.

D. Discussion

It can be found that there are $N \times K$ phase shifts required. Although many phase shifters are required, it is a mature structure that for example has been widely used in the analog precoder part of hybrid beamforming [36]. Thus the phase matrix is practically available in hardware. Since the contribution of this paper is for the testing at sub-6GHz frequency band, where the massive MIMO bast station could provide antenna connectors for connective testing [15-17], the proposed conductive technique is feasible. Although the antenna connector is available, the traditional full conductive testing solution is inapplicable for the massive MIMO BS due to the high costs. Therefore the proposed methodology is a promising solution, since the required phase shifters are much cheaper compared with the CE resources. By adding the phase shifter matrix, we can significantly reduce the required CE resources, while achieving the same purpose. On the other hand, for testing at millimeter wave band where the antenna connectors are not accessible or sub-6GHz bands where we have integrated RF transceiver design, the wireless cable method can be considered to enable the function of RF cable in a radiated manner [35]. In the ideal case, the wireless cable between the nth output of the phase matrix and the nth DUT antenna can be enabled without any cross-talking, as if the phase matrix and the DUT are directly connected [37]. This wireless cable method will be our further research.

III. Virtual OTA Setup

A. System Model

For a typical massive MIMO array with 3D beamforming, a set of complex weights will be applied to the array antennas to form a beam focusing on a certain direction according to the array factor depending on the channel propagation geometry. To test 5G gNodeB's (gNBs), the DUT should observe the emulated paths exhibiting spatial profiles similar to that of the target channel. For the channel emulation with the conductive phase matrix setup, the overall system model is:

$$\boldsymbol{y}(f,t) = \boldsymbol{F}(f,t)\boldsymbol{H}_{OTA}(f,t)\boldsymbol{x}(f,t), \tag{1}$$

The phase matrix connecting the K virtual probes to the N receive antennas can be expressed as $\boldsymbol{F}(f,t) = \{\gamma_{n,k}\} \in \mathbb{C}^{N\times K}$, where $\gamma_{n,k} = e^{j(\boldsymbol{\beta_k}\cdot\boldsymbol{r_n})}$, and $\boldsymbol{\beta_k}$ is the wave vector from the spatial direction characterizing the kth virtual probe. $\boldsymbol{r_n}$ is the location vector of the nth DUT antenna. Practically, the phase matrix is frequency and time invariant, and therefore $\boldsymbol{F}(f,t) = \boldsymbol{F}$ [16]. This system model is similar to the hybrid beamforming in form [15], while the purpose and processing algorithm are different [16] [38].

B. Channel emulation

As discussed in [39] and [40], for the DUT with limited spatial resolution, the experienced channel spatial characteristics in the target environment can be reproduced by a few significant paths. In other words, the channel to be emulated can be represented by a few spatial paths, which can be considered as the partial spatial sampling method [16]. Since an arbitrary single path can be modelled by each of the inputs of the phase matrix as shown in Fig. 2, the spatial characteristic emulation can be considered as a sparse recovery problem which is to reconstruct the whole target spatial profile with a limited number of paths with specific directions and powers. Spatial correlation, measuring the statistical signal similarity at different antennas, is generally used to assess how well the

spatial profiles are emulated, and is Fourier transform pair with the target channel PAS [11]:

$$\rho_i = \oint P(\Omega)\exp(j\frac{2\pi}{\lambda}\boldsymbol{\Omega}(\boldsymbol{r}_{i,u} - \boldsymbol{r}_{i,v})), \tag{2}$$

ρ_i is the spatial correlation for the ith antenna pair composing of the uth and the vth antennas. λ is the wavelength. $\boldsymbol{\Omega}$ is the unit direction vector of the solid angle Ω. The spatial correlation generated with a limited number of paths, $\hat{\rho}_i$, can be calculated as [40]:

$$\hat{\rho}_i = \sum_{k=1}^{K} g_k \exp(j\frac{2\pi}{\lambda}\boldsymbol{\Phi}_k(\boldsymbol{r}_{i,u} - \boldsymbol{r}_{i,v})), \tag{3}$$

$\boldsymbol{\Phi}_k$ and g_k are the unit position vector and power weight of the kth path. For *K* paths at given positions, the path powers $\boldsymbol{g} = \{g_k\} \in \mathbb{C}^{K\times 1}$ can be obtained by solving the following objective function:

$$\boldsymbol{g} = \arg\min \| \hat{\boldsymbol{\rho}}(\boldsymbol{g}, \boldsymbol{\phi}) - \boldsymbol{\rho} \|_2^2, \tag{4}$$

$\| \cdot \|_2$ is the 2-norm operation. $\boldsymbol{\rho} = \{\rho_i\} \in \mathbb{C}^{Q\times 1}$ and $\hat{\boldsymbol{\rho}} = \{\hat{\rho}_i\} \in \mathbb{C}^{Q\times 1}$ are the target and the generated channel spatial correlation vectors, respectively. Here are $Q = N^2$ antenna pairs of any two antennas among the N array elements. $\boldsymbol{\phi} = \{\Phi_k\} \in \mathbb{C}^{K\times 1}$ is the vector containing the path directions. Note that g_k should be the real number as the phase variation is implemented in phase matrix.

Since the required number of CE outputs, i.e. *K*, is the key cost-determining factor, we aim to optimize the virtual probe configuration to achieve satisfying emulation accuracy with limited CE resources. Obviously, the emulation accuracy relies on the spatial locations and power weights of the virtual probes. Although (3) and (4) are similar to the forms of the PFS technique in MPAC [41], the previous solutions to calculate the optimal probe locations and power weights are not suitable to the conductive phase matrix method for a non-stationary environment. Since more possible probe locations are expected in the virtual OTA setup, the mentioned probe selection algorithms in MPAC would necessitate more redundant calculation of all possible probe contributions in channel emulation. Another problem is the virtual probe weight computation, where the generally used numerical optimization method with convex optimization is too time-consuming for dynamic channel emulation. In this work, we aim to address these two problems, i.e. the probe location and probe weight determination for the virtual MPAC setup.

IV. Virtual Probe Configuration

A. State-of-the-art

In [16], the virtual probes are determined in the directions of the two strongest clusters of the target channel. In [35], the SAM algorithm in the MPAC is embedded into the virtual setup: i.e. to allocate the probes to the directions of clusters, in order of power. Convex optimization is the widely used method to obtain the probe power weights by solving (4) when the probe locations are determined. Although a direct sampling method was proposed in [11], it offers limited emulation accuracy and therefore is not applicable for massive MIMO dynamic channel emulation. Furthermore, the existing solutions are for the cluster-based standard channels and are not suitable to emulate channels at each snapshot.

B. Power Weight Computation

To solve (4) in a highly efficient way, a simple closed-form power weighting formulation is derived. $\hat{\boldsymbol{\rho}}$ in (5) can be rewritten as $\hat{\boldsymbol{\rho}} = \boldsymbol{A} \cdot \boldsymbol{g}$ where we have $\boldsymbol{A} = [\boldsymbol{a_1}, ..., \boldsymbol{a_K}] \in \mathbb{C}^{Q\times K}$ with $\boldsymbol{a_k} = [\exp(j\frac{2\pi}{\lambda}\boldsymbol{\Phi}_k(\boldsymbol{r}_{1,u'} - \boldsymbol{r}_{1,v'})), ..., \exp(j\frac{2\pi}{\lambda}\boldsymbol{\Phi}_k(\boldsymbol{r}_{Q,u} - \boldsymbol{r}_{Q,v}))]^T \in \mathbb{C}^{Q\times 1}$. The real parts of $\boldsymbol{\rho}$ and $\boldsymbol{A}$ are defined as $\boldsymbol{\rho}_{Re}$ and $\boldsymbol{A}_{Re}$, respectively. The imaginary parts of $\boldsymbol{\rho}$ and $\boldsymbol{A}$ are defined as $\boldsymbol{\rho}_{Im}$ and $\boldsymbol{A}_{Im}$, respectively. Define $L = \|\hat{\boldsymbol{\rho}} - \boldsymbol{\rho}\|_2^2$, and it can be written as:

$$L = \|\boldsymbol{A}_{Re} \cdot \boldsymbol{g} - \boldsymbol{\rho}_{Re}\|_2^2 + \|\boldsymbol{A}_{Im} \cdot \boldsymbol{g} - \boldsymbol{\rho}_{Im}\|_2^2. \tag{5}$$

Then we can take the derivative of L:

$$\frac{\partial L}{\partial \boldsymbol{g}} = 2(\boldsymbol{A}_{Re}^T \cdot \boldsymbol{A}_{Re} \cdot \boldsymbol{g} - \boldsymbol{A}_{Re}^T \cdot \boldsymbol{\rho}_{Re} + \boldsymbol{A}_{Im}^T \cdot \boldsymbol{A}_{Im} \cdot \boldsymbol{g} - \boldsymbol{A}_{Im}^T \cdot \boldsymbol{\rho}_{Im}). \tag{6}$$

Make $\frac{\partial L}{\partial \boldsymbol{g}} = 0$ then we can obtain:

$$\boldsymbol{g} = (\boldsymbol{A}_{Re}^T \cdot \boldsymbol{A}_{Re} + \boldsymbol{A}_{Im}^T \cdot \boldsymbol{A}_{Im})^{-1} \cdot (\boldsymbol{A}_{Re}^T \cdot \boldsymbol{\rho}_{Re} + \boldsymbol{A}_{Im}^T \cdot \boldsymbol{\rho}_{Im}). \tag{7}$$

Using (7), we can obtain the power weights in a simple and computationally efficient manner. Furthermore, the obtained power weights are real numbers. Since (5) is a convex function, the power weights making $\frac{\partial L}{\partial \boldsymbol{g}} = 0$ should be the optimal result minimizing L without constraint. In the following algorithm to determine the probe location, (7) is used to determine the probe weights as discussed later.

C. Successive probe determination

Different from the traditional algorithms, the proposed algorithm determines the probe location from the estimated PAS. Using the classical Bartlett beamformer [42] for the target and the emulated channel, the PAS seen (estimated) by the DUT, respectively are:

$$\hat{P}_T(\Omega) = \boldsymbol{a}^H(\Omega)\boldsymbol{R}\boldsymbol{a}(\Omega) \tag{8}$$

$$\hat{P}_O(\Omega) = \boldsymbol{a}^H(\Omega)\hat{\boldsymbol{R}}\boldsymbol{a}(\Omega) \tag{9}$$

$\boldsymbol{R} = \{\rho_i\} \in \mathbb{C}^{N\times N}$ and $\hat{\boldsymbol{R}} = \{\hat{\rho}_i\} \in \mathbb{C}^{N\times N}$ are the target and the emulated spatial correlation matrices, respectively. $\boldsymbol{a}(\Omega)$ is the steering vector of DUT array. Since the emulated spatial correlation can be decomposed into the form of coherent superposition with (3), (9) can be rewritten as:

$$\hat{P}_O(\Omega) = \boldsymbol{a}^H(\Omega)[\hat{\boldsymbol{R}}_1 + \hat{\boldsymbol{R}}_2 + ... + \hat{\boldsymbol{R}}_K]\boldsymbol{a}(\Omega) \tag{10}$$

$\hat{\boldsymbol{R}}_k$ is the partial spatial correlation emulated by the kth operating probe. Inspired by the SC principle, we can extract dominant channel path parameters in a successive manner as detailed in the following procedure:

1) For the target channel to be emulated, calculate the spatial correlation at DUT based on (2). Applying (8), we can define the current residual PAS as $\boldsymbol{r}_1 = \hat{P}_T(\Omega)$. Define $l = 1$.

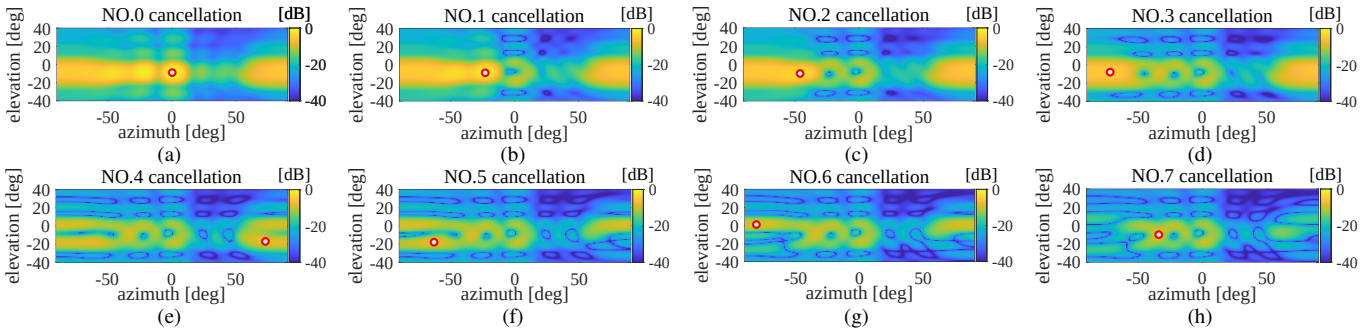

Fig. 3. The implementation of the probe determination procedures. The white dot with red border is the probe location to be selected in each cancellation.

Algorithm 1: The proposed algorithm

Input: K, target spatial correlation matrix $\boldsymbol{R}$.

initialization: Initial residual PAS: $\boldsymbol{r}_1 = \hat{P}_T(\Omega)$. Define $l = 1$;

while $l \leq K$ **do**

  Set the lth virtual probe to be placed at $\widetilde{\Phi}_l$ which presents the peak power value in $\boldsymbol{r}_l$;

  Calculate the current estimated PAS $\hat{P}_O(\Omega)$ with the l determined virtual probes based on (3)(7)(9);

  Update the residual PAS $\boldsymbol{r}_{l+1} = \hat{P}_T(\Omega) - \hat{P}_O(\Omega)$, $l = l + 1$.

end

Output: $\widetilde{\boldsymbol{\phi}} = \{\widetilde{\Phi}_1, \widetilde{\Phi}_2, ..., \widetilde{\Phi}_K\}$.

2) Detect the spatial position which presents the peak power in $\boldsymbol{r}_l$, and a new virtual probe is determined to be located at this detected spatial position.
3) Calculate the power weights for the l already determined probes via (7). Then the emulated spatial correlation as well as the estimated PAS $\hat{P}_O(\Omega)$ can be obtained based on (3) and (9).
4) Update $\boldsymbol{r}_{l+1} = \hat{P}_T(\Omega) - \hat{P}_O(\Omega)$, and $l = l + 1$.
5) Repeat procedures 2-4 until K probes are selected.

With the principle of SC, we remove (cancel) the effects of the already determined probes to obtain the residual PAS, and then the optimal probe location can be straightforwardly found in $\boldsymbol{r}_l$. The procedures of the proposed virtual probe location determination method are summarized in Algorithm 1. To make the proposed algorithm more readable, Fig. 3 presents an example process of determining $K = 8$ probes, where the DUT is an 8×8 array with 0.5λ spacing and the 3GPP 38.901 clustered delay line (CDL)-C model [43] is considered the target channel.

Note that with (7), the practical constraint [44] of $\|\boldsymbol{g}\|_1 = 1$ is not satisfied, where $\|\cdot\|_1$ is 1-norm operation. The actual objective function to calculate the final power weights should be:

$$\min L(\boldsymbol{g}). \quad s.t.\ \|\boldsymbol{g}\|_1 = 1. \tag{11}$$

Naturally it can be deduced that directly performing normalization $\boldsymbol{g} = \boldsymbol{g}/\|\boldsymbol{g}\|_1$ for (7), after probe determination, can not minimize L. For this reason, a novel weight normalization method which can obtain the optimal normalized power weight is proposed here. Specifically, for this constrained linear regression problem, the Lagrange multiplier method can be employed and a new objective function can be structured:

$$T = \|\boldsymbol{A_{Re}} \cdot \boldsymbol{g} - \boldsymbol{\rho}_{Re}\|_2^2 + \|\boldsymbol{A}_{Im} \cdot \boldsymbol{g} - \boldsymbol{\rho}_{Im}\|_2^2 + \alpha(\|\boldsymbol{g}\|_1 - 1), \tag{12}$$

where α is a hyper-parameter. According to the Lagrange multiplier method [45] which is used to the calculate the optimal result for constrained regression problem, the power weights minimizing T satisfy (11) as well. Specificity, the following equations should be satisfied:

$$\begin{cases} \frac{\partial T}{\partial \boldsymbol{g}} = 0 \\ \frac{\partial T}{\partial \alpha} = 0 \end{cases}. \tag{13}$$

With (13), we can obtain:

$$\boldsymbol{g} = (\boldsymbol{A}_{Re}^T \cdot \boldsymbol{A}_{Re} + \boldsymbol{A}_{Im}^T \cdot \boldsymbol{A}_{Im})^{-1} \cdot (\boldsymbol{A}_{Re}^T \cdot \boldsymbol{\rho}_{Re} + \boldsymbol{A}_{Im}^T \cdot \boldsymbol{\rho}_{Im} - \frac{\alpha \boldsymbol{I}}{2}), \tag{14}$$

where $\boldsymbol{I} = [1, ...1]^T \in \mathbb{C}^{K \times 1}$ is a column vector. In addition, α can be computed as:

$$\alpha = \frac{2 \cdot \boldsymbol{I}^T (\boldsymbol{A}_{Re}^T \cdot \boldsymbol{A}_{Re} + \boldsymbol{A}_{Im}^T \cdot \boldsymbol{A}_{Im})^{-1} (\boldsymbol{A}_{Re}^T \cdot \boldsymbol{\rho}_{Re} + \boldsymbol{A}_{Im}^T \cdot \boldsymbol{\rho}_{Im}) - 2}{\boldsymbol{I}^T (\boldsymbol{A}_{Re}^T \cdot \boldsymbol{A}_{Re} + \boldsymbol{A}_{Im}^T \cdot \boldsymbol{A}_{Im})^{-1} \boldsymbol{I}}, \tag{15}$$

(14) and (15) are closed-form results as well, and can be computed with low computational complexity. More importantly, since (12) is a convex function, the local optimum is the global optimum. Thus (14) is the optimal power weights minimizing the objective function (11) with the constrain of $\|\boldsymbol{g}\|_1 = 1$, and it is the identical result compared with that obtained with the complicated convex numerical optimization algorithm. Since $g_k \in \boldsymbol{g}$ should be a positive number (negative number means the kth probe can not contribute to channel emulation and will not be determined), the constrain of $g_k > 0$ [44] is not discussed.

V. Algorithm Validation

A. Simulation channels

In this section, the performance for channel model emulation is examined with our proposed virtual probe configuration methodologies. The previously used 8×8 array is assumed to be the DUT. For comparison, three popular algorithms

TABLE I
ALGORITHM COMBINATION.

configuration	Probe locating method	Probe weighting method
D1	SAM	convex optimization
D2	proposed method	proposed method
D3	proposed method	convex optimization
D4	PSO	convex optimization

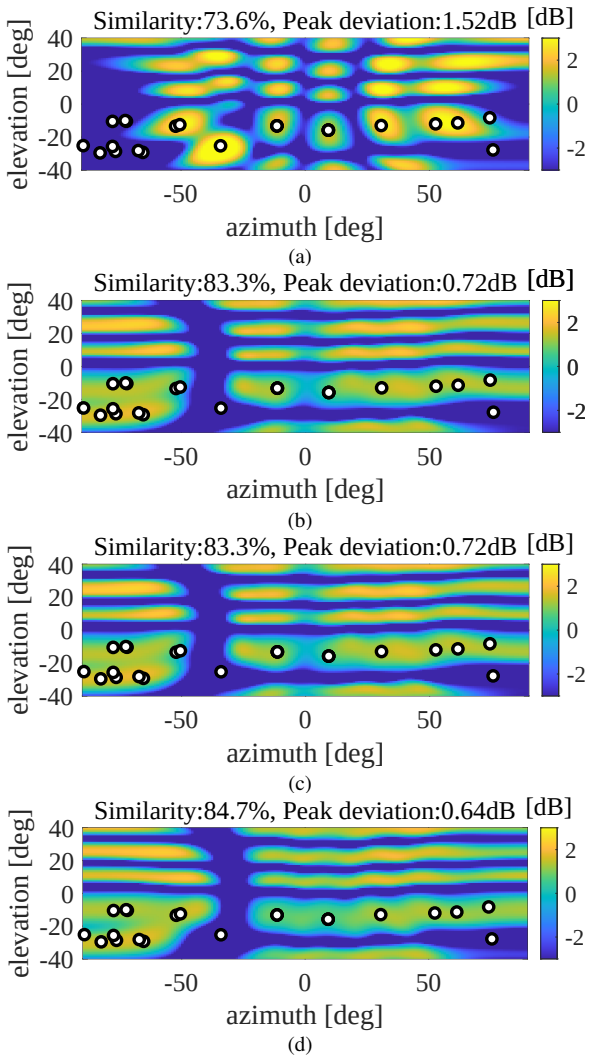

Fig. 4. Emulation deviation of the estimated PAS from the target with (a) D1, (b) D2, (c) D3 and (d) D4 configurations. The dot with black border are the cluster locations.

are implemented and compared. The algorithm combinations are shown in Table. I, where the particle swarm optimization (PSO) [33] is run several times to avoid local optima, and the probe location set, minimizing the weighted root mean square (RMS) spatial correlation error [11], is set to be the final location. The metric of PAS similarity is defined in [11]. Peak deviation refers to the power deviation between $\hat{P}_O(\Omega)$ and $P_T(\Omega)$ at the direction where the target strongest beam is located. Note that though the 3GPP CDL channel profile is not defined for each snapshot but at the cluster level, it provides a good reference for the algorithm validation and is therefore utilized here.

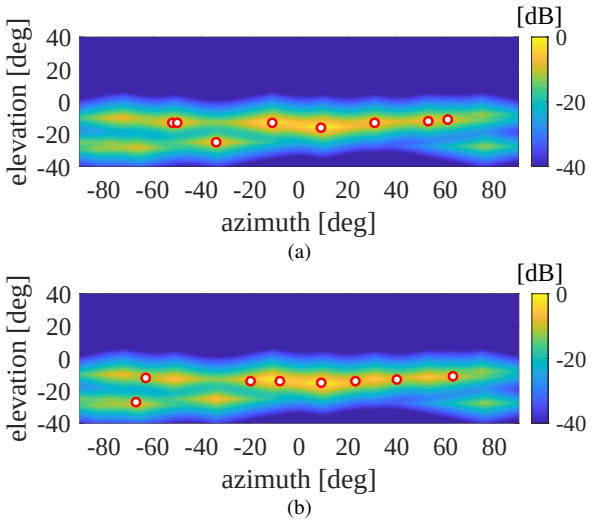

Fig. 5. Probe layouts determined by (a) D1, and (b) D2, respectively.

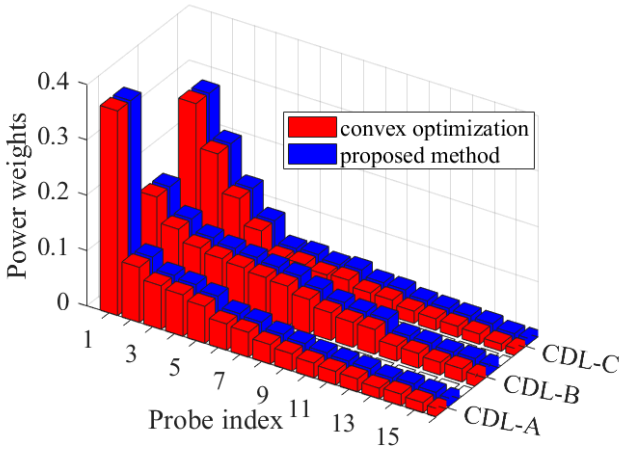

Fig. 6. The comparison of the power weighs obtained form different methods for various channel models.

1) PAS emulation: In the virtual OTA case where all the discussed configurations are implemented with 8 virtual probes, the PAS deviations between $\hat{P}_O(\Omega)$ and $P_T(\Omega)$ estimated with DUT are shown in Fig. 4, where the CDL-B model is set as the target channel. It can be found that the proposed methodologies D2 exhibit satisfying performance comparable to that of D4, where PSO should be the most accurate algorithm besides the brute force method [30]. Furthermore, Fig. 4 (b) and (c) show identical results, whether in terms of the PAS similarity or the peak deviation. It implies that there is no penalty on accuracy due to the proposed closed-form weighting strategy. Regarding D1, larger deviations can be observed, and more PAS deviations appear in the region where some clusters are located, resulting in an undesired result. Fig. 5 shows the probe layouts determined with SAM and the proposed method for the CDL-B model. In addition, if we adopt the direct sampling method in [11] for D1, the PAS similarity and peak deviation will further degrade to 72.8% and 2.7dB. Particularly, Fig. 6 presents in D2 and D3 cases the power weights for 16 virtual probes to reconstruct different channel models. It indicates that the proposed power weighting method provides the same power weight coefficients as that

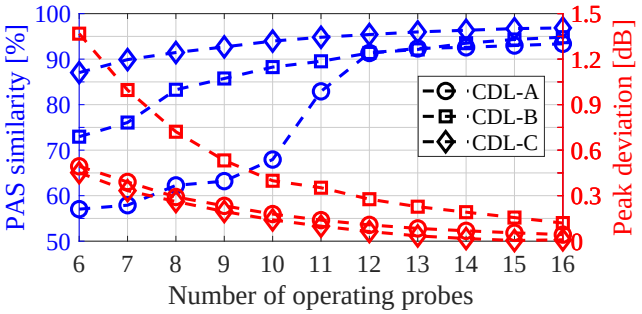

Fig. 7. Estimated PAS deviation emulated with various numbers of operating probes, for diverse channel models, in D2 case.

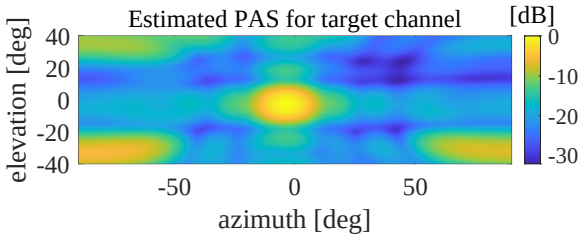

Fig. 8. Estimated PAS for the target CDL-A channel model.

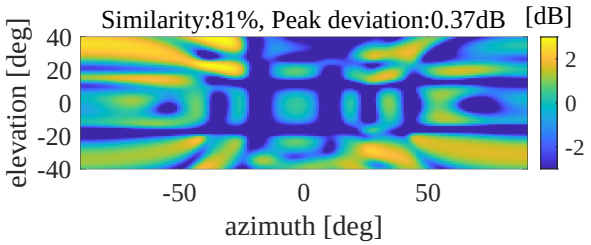

Fig. 9. Emulation deviation of the estimated PAS from the target with D2 using angle spacing limit.

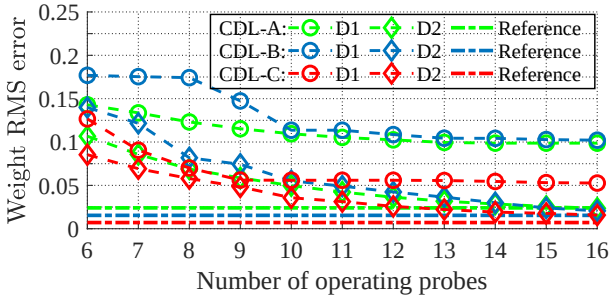

Fig. 10. Weighted RMS correlation error emulated with various numbers of operating probes, for diverse channel models, in D1 and D2 cases.

obtained with the convex optimization algorithm, guaranteeing the emulation accuracy.

To examine the robustness of our proposed algorithms, three representative channel models, CDL-A, B, C, are emulated with various numbers of virtual operating probes. Fig. 7 shows that with 12 probes at least 91% PAS similarity and 0.28dB peak deviation can be achieved. The proposed algorithm combination presents the best performance for the CDL-C model, since the cluster angle spread is very small which leads to relatively distinct power in the PAS. In contrast, with regard to the CDL-B model, since the cluster power is relatively average and is distributed in a large region, the peak deviation exceeding 1dB can be observed with 6 probes.

However, regarding the CDL-A model, performance degeneration in terms of PAS similarity can be observed when the number of operating probes is small. It is because the CDL-A model is not very directive, with rich multi-path in the space. Not only a large beam exists with concentrated power as shown in Fig. 8, but also many clusters with small power are distributed in a quite wide range. Thus, more operating probes are required. When using a small number of probes, the probes are preferentially determined to reduce the peak deviation with less consideration given to the PAS similarity. In other words, the virtual probes are mainly deployed in the center. To handle these problems, the angular spacing limit can be introduced in the proposed method: the new probes to be determined can not be laid out at an angle whose angular distances from the already determined probes are less than the threshold value δ. Fig. 9 shows the emulation deviation for the CDL-A model with 8 virtual probes in the D2 case when $\delta = 20°$, while the PAS similarity and peak deviation are 68.9% and 0.42dB in the D1 case. Angular spacing limit is a simple mean to force the probes to be deployed more widely and to give more consideration to the PAS similarity when the number of operating probes is small.

2) Spatial correlation emulation: Furthermore, since spatial correlation plays an important role in MIMO spatial multiplexing, the weighted RMS correlation error is another crucial metric to assess how well the propagation channel is reconstructed. In D1 and D2 cases, Fig. 10 shows the weight RMS correlation error emulated with various numbers of probes, where references are the results emulated with D4 algorithms using 16 probes. It can be found that with the proposed methodologies, the emulation accuracy approaches that of D4. In contrast, the weight RMS errors in the D1 case are ineffectively improved with more operating probes, due to the limitation of the SAM method. Thus more advantageous performances of D2 are convincingly demonstrated compared with D1.

3) Discussion: Note that convex optimization, though widely used in the literature, is actually not applicable in practical dynamic channel emulation, due to the computational complexity. However, our proposed closed-form power weighting strategy provides the same optimal accuracy as that offered by the convex optimization method, while it can be implemented with high computational efficiency. On the other hand, in the process of implementing the proposed probe determination algorithm which exhibits satisfying performance, there is no need for numerical optimization as well, and it is advantageous compared with the traditional probe selection algorithm in MPAC. Note that the proposed methodologies can be applied to not only the investigated virtual OTA setup, but also the actual MPAC system.

B. Measured realistic channel emulation

Different from the standard channel model, the measured site or route-specific channel is more versatile and realistic.

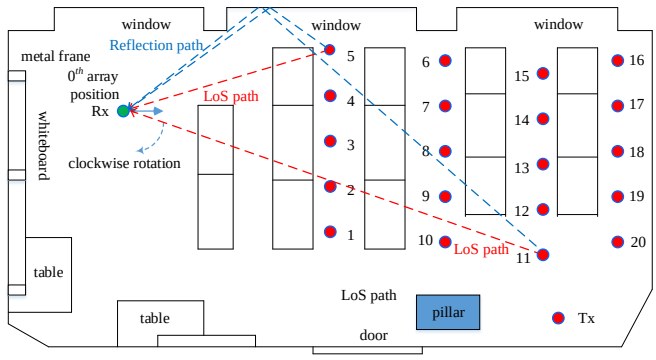

(a)

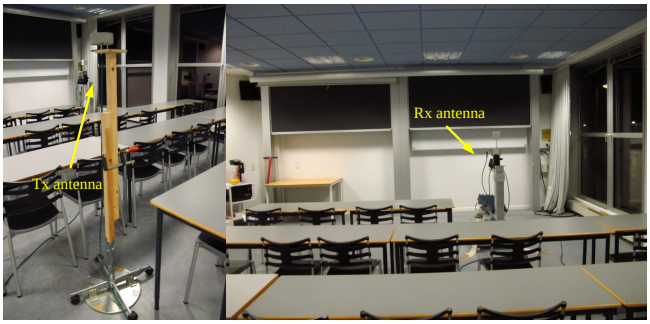

(b)

Fig. 11. (a) The geometric layout of the classroom measurement scenario. (b) The photograph of the measurement scenario and Tx (left), Rx (right) antennas.

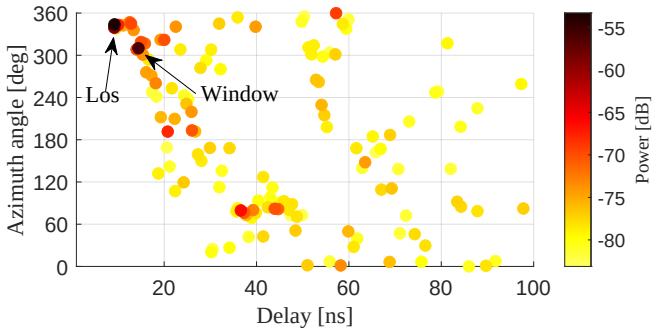

Fig. 12. The estimated PDAS at position 5.

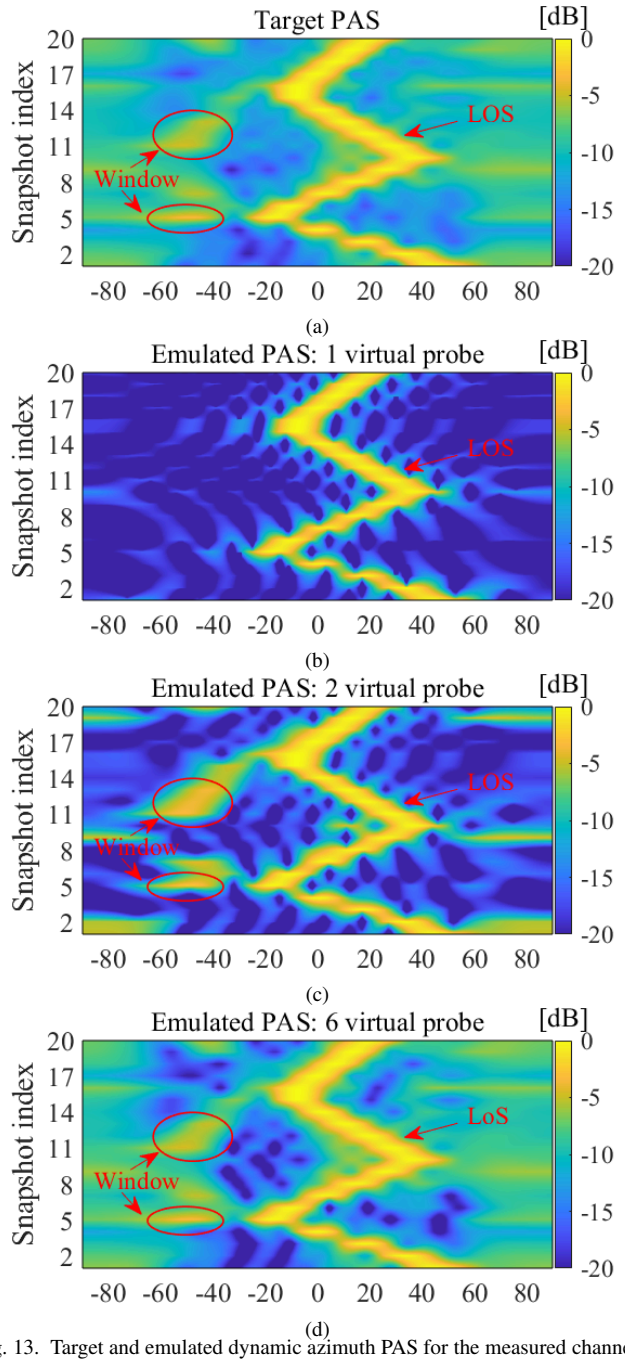

(a) (b) (c) (d)

Fig. 13. Target and emulated dynamic azimuth PAS for the measured channel. (a) Target PAS. (b) 1 virtual probe. (c) 2 virtual probe. (d) 6 virtual probe.

Thus, the feasibility and applicability of our proposed methods for emulating the measured channel are validated.

1) Measurement campaign and parameter estimation: A measurement campaign in the indoor classroom at 2-4 GHz was conducted to obtain the dynamic channel evolution behaviors. To be specific, a virtual uniform circular array (UCA)-based vector network analyzer (VNA) ultra-wideband channel sounding system [46] is utilized for the measurements. Two quasi-omnidirectional biconical antennas are exploited as the transmitter and receiver antennas, respectively. The Rx antenna is clockwise rotated at a pre-set radius of $r = 0.24$m from the $0th$ position to form a virtual UCA containing $E = 360$ elements. The holistic measurement scenario is depicted in Fig. 11 including the Tx, Rx, as well as the surroundings. The dimension of the indoor environment is $8.54 \times 6.70 \times 2.71\text{m}^3$. In the measurement scenario, the main surroundings are wooden tables and chairs, concrete walls and floors, blackboard, and glass windows, and the material properties of which are discussed in [47]. Both Tx and Rx antennas are set with the height of 1.50m. 20 measurement points with the spacing of 0.8m by moving the Tx in each row were measured sequentially. Readers are referred to [48] for more measurement and system details. At each Tx point, 750 frequency points were recorded for the E elements in virtual UCA. Based on the measured channel transfer functions (CTFs) at each Tx location, a high-resolution estimation algorithm [49] is applied to estimate the multipath component (MPC) propagation parameters, i.e. path delays, azimuth angles, elevation angles, and complex amplitudes.

Position 5 in Fig. 11 alongside the window is regarded

as a typical position and the corresponding estimated power-delay-azimuth spectrum (PDAS) is presented in Fig. 12. Due to the limited aperture of the used virtual UCA in the elevation domain, only the azimuth angle is considered for the channel parameters. According to the geometric layout of the measurement scenario as well as the channel propagation parameters, the main paths radiated from two positions are drawn as examples. It can be found that the strong paths are contributed by the LOS which is not considered in simulation with standard channel models, and the reflections from the window, respectively. As shown in Fig. 12, there are no distinct boundaries between MPCs, and a complicated high-resolution clustering solution is required for the existing algorithms. Thus, the conductive phase matrix method and our proposed probe determination methodology are advantageous to emulate channels at the snapshot level, since they are insusceptible to the cluster definition.

2) Emulation for the measured dynamic channel: $K = 1, 2, 6$ virtual probes are used to emulate this measured dynamic channel. Fig. 13 illustrates the azimuth PAS evolution behavior sliced in the target and the emulated cases. The previously used 8×8 array is used as the DUT. Since this DUT can not distinguish the paths symmetrical about the array plane, the presented PAS is limited from -90° to 90°. Note that the PAS power has been normalized at each snapshot. Since the LOS path is dominant, the PAS similarity up to 82.8% can be achieved with 1 virtual probe. In Fig. 13 (b) the evolution trajectory of the LOS path is reproduced accurately. Using 2 virtual probes, the main reflection paths can be emulated. As shown in Fig. 13 (c), the reflections caused by the window for position 5 are also exhibited, and are consistent with the results in Fig. 12. Furthermore, the "birth-death" behaviors of clusters along the measurement route can be observed and the evolution is consistent with the target. To emulate more weak clusters, more virtual probes are employed. It can be found in Fig. 13 (d) that the emulated azimuth PAS with 6 virtual probes matches well with the target, where the peak deviation and PAS similarity are 0.1dB and 95%, respectively. Meanwhile, the maximum weighted RMS correlation error for all positions is only 0.04.

VI. Conclusion

In this paper we sketched the principle of a conductive massive MIMO testing method that combines the CE and phase matrix to emulate fading channel in a cost-effective way. For the dynamic channel emulation for massive MIMO beamforming evaluation, this paper presents a novel accurate, and computation-efficient scheme to determine the locations and power weights for virtual probes.

For the standard 3GPP 38.901 CDL channel models, we have performed comprehensive simulations to examine the performance of our proposed methods. For instance, with 12 virtual probes, more than 91% PAS similarity can be achieved. Furthermore, it is shown that the proposed closed-form power weighting strategy presents identical results compared with the convex optimal algorithm, yet with significantly reduced computational complexity, which is key to dynamic channel emulation. To assess our proposed methodologies more practically, the measured dynamic channel is emulated with the proposed methods. Using 6 virtual probes both the LOS and the reflection paths can be accurately reconstructed as well.

References

[1] E. G. Larsson, O. Edfors, F. Tufvesson, and T. L. Marzetta, "Massive MIMO for next generation wireless systems," *IEEE Commun. Mag.*, vol. 52, no. 2, pp. 186–195, Feb. 2014.

[2] X. Zhao, A. M. A. Abdo, C. Xu, S. Geng, J. Zhang, and I. Memon, "Dimension reduction of channel correlation matrix using CUR-decomposition technique for 3-D massive antenna system," *IEEE Access*, vol. 6, pp. 3031–3039, Dec. 2017.

[3] M. Wang, C. Zhang, X. Chen and S. Tang, "Performance Analysis of Millimeter Wave Wireless Power Transfer With Imperfect Beam Alignment," *IEEE Tran. Veh. Technol.*, vol. 70, no. 3, pp. 2605-2618, Mar. 2021.

[4] X. Zhao, A. M. A. Abdo, Y. Zhang, S. Geng, and J. Zhang, "Single RFchain beam training for MU-MIMO energy efficiency and informationcentric IoT millimeter wave communications," *IEEE Access*, vol. 7, pp. 6597–6610, Dec. 2019.

[5] "Verification of radiated multi-antenna reception performance of User Equipment," 3GPP, TR 37.977 V1.0.0, Sep. 2013.

[6] P. Kyösti, T. Jämsä, and J.-P. Nuutinen, "Channel modelling for multiprobe over-the-air MIMO testing," *International Journal of Antennas and Propagation*, vol. 2012, Art. no. 615954, Mar. 2012.

[7] H. Pei, X. Chen, W. Fan, M. Zhang, A. Zhang, and T. Svensson, "Comparisons of channel emulation methods for state-of-the-art multi-probe anechoic chamber based millimeter-wave over-the-air testing," *IEEE VTC-Fall*, Honolulu, HI, Sep. 2019, pp. 1–5.

[8] 3GPP TR 37.977, "Universal Terrestrial Radio Access (UTRA) and Evolved Universal Terrestrial Radio Access (E-UTRA); Verification of radiated multi-antenna reception performance of User Equipment (UE)," V16.0.0, July 2020.

[9] 3GPP, "Study on radiated metrics and test methodology for the verification of multi-antenna reception performance of nr user equipment (ue);," Jun. 2020.

[10] 3GPP TR 38.827, "Study on radiated metrics and test methodology for the verification of multi-antenna reception performance of NR User Equipment (UE)," V16.4.0, September 2021.

[11] P. Kyösti, L. Hentilä, W. Fan, J. Lehtomäki, and M. Latva-Aho, "On radiated performance evaluation of massive MIMO devices in multi-probe anechoic chamber OTA setups," *IEEE Trans. Antennas Propag.*, vol. 66, no. 10, pp. 5485–5497, Oct. 2018.

[12] P. Kyösti, W. Fan, G. F. Pedersen, and M. Latva-aho, "On dimensions of OTA setups for massive MIMO base stations radiated testing," *IEEE Access*, vol. PP, no. 99, pp. 1–1, 2016.

[13] P. Kyösti, L. Hentilä, J. Kyröläinen, F. Zhang, W. Fan, and M. Latvaaho, "Emulating dynamic radio channels for radiated testing of massive MIMO devices," in *Proc. 12th Eur. Conf. Antennas Propag. (EuCAP)*, Apr. 2018, pp. 1–5.

[14] Q. Zhu, H. Li, Y. Fu, C.-X. Wang, Y. Tan, X. Chen, and Q. Wu, "A novel 3D non-stationary wireless MIMO channel simulator and hardware emulator," *IEEE Trans. Commun.*, vol. 66, no. 9, pp. 3865–3878, Sep. 2018.

[15] D. Reed, A. Rodrguez-Herrera, and J. P. Nuutinen, "Massive MIMO array testing using a programmable phase matrix and channel emulator," in *Proc. 12th Eur. Conf. Antennas Propag. (EUCAP)*, Apr. 2018, pp. 1–4.

[16] P. Kyösti and P. Heino, "Fading Channel Emulation for Massive MIMO Testing Using a Conductive Phase Matrix Setup," in *Proc. 14th Eur. Conf. Antennas Propag. (EUCAP)*, Mar. 2020, pp. 1–4.

[17] W. Fan, L. Hentilä, F. Zhang, P. Kyösti, and G. F. Pedersen, "Virtual drive testing of adaptive antenna systems in dynamic propagation scenarios for vehicle communications," *IEEE Access*, vol. 6, pp. 7829–7838, Jan. 2018.

[18] L. Hentilä, P. Kyösti, and P. Heino, "Evaluation of beam forming and multi antenna techniques in non-stationary propagation scenarios with HW emulator," in *Proc. Int. ITG Workshop Smart Antennas (WSA)*, Mar. 2012, pp. 347–351.

[19] Z. Ma, B. Ai, R. He, Z. Zhong and M. Yang, "A non-stationary geometry-based MIMO channel model for millimeter-wave UAV networks," *IEEE J. Sel. Areas Commun.*, vol. 39, no. 10, pp. 2960-2974, Oct. 2021.

[20] P. Qi, Y. Zhang, Z. Yuan, L. Yu, P. Tang, and J. Zhang, "Channel modeling based on 3D scenario information for V2I communications," in *Proc. 15th Eur. Conf. Antennas Propag. (EuCAP)*, 2021, pp. 1–5.
[21] Y. Li, R. He, S. Lin, K. Guan, D. He, and Q. Wang, "Cluster-based nonstationary channel modeling for vehicleto-vehicle communications," *IEEE Antennas Wireless Propag. Lett.*, vol. 16, pp. 408–411, Nov. 2017.
[22] Q. Zhu, Y. Yang, X. Chen, Y. Tan, Y. Fu, C.-X. Wang, and W. Li, "A novel 3D non-stationary vehicle-to-vehicle channel model and its spatial-temporal correlation properties," *IEEE Access*, vol. 6, pp. 43633–43643, Jul. 2018.
[23] Z. Ma, B. Ai, R. He, G. Wang, Y. Niu, and Z. Zhong, "A wideband nonstationary air-to-air channel model for UAV communications," *IEEE Trans. Veh. Technol.*, vol. 69, no. 2, pp. 1214–1226, Feb. 2019.
[24] P. Shen, Y. Qi, W. Yu, F. Li, X. Wang and X. Shen, "A Directly Connected OTA Measurement for Performance Evaluation of 5G Adaptive Beamforming Terminals," *IEEE Internet Things J*, doi: 10.1109/JIOT.2022.3150038.
[25] S. Jacobsson, G. Durisi, M. Coldrey, U. Gustavsson, and C. Studer, "Throughput analysis of massive MIMO uplink with low-resolution ADCs," *IEEE Wireless Commun.*, vol. 16, pp. 4038–4051, Jun. 2017.
[26] H. Lin, F. Gao, S. Jin, and G. Y. Li, "A new view of multi-user hybrid massive MIMO: Non-orthogonal angle division multiple access," *IEEE J. Sel. Areas Commun.*, vol. 35, no. 10, pp. 2268–2280, Oct. 2017.
[27] C. Schirmer, M. H. Landmann, W. A. T. Kotterman, M. Hein, R. S. Thom¨a, G. D. Galdo, and A. Heuberger, "3D wave-field synthesis for testing of radio devices," in *Proc. 8th Eur. Conf. Antennas Propag. (EUCAP)*, Apr. 2014, pp. 3394–3398.
[28] C. Schirmer, A. Rügamer, W. A. T. Kotterman, M. H. Landmann, and G. Del Galdo, "Evaluation of array antenna systems for GNSS applications using wave-field synthesis in an OTA laboratory," in *Proc. 11th Eur. Conf. Antenna Propag. (EUCAP)*, Mar. 2017, pp. 2029–2032.
[29] W. Fan, P. Kyösti, M. Rumney, X. Chen and G. F. Pedersen, "Over the-air radiated testing of millimeter-wave beam-steerable devices in a cost-effective measurement setup," *IEEE Commun. Mag.*, vol. 56, no. 7, pp. 64–71, Jul. 2018.
[30] W. Fan, F. Sun, J. Ø. Nielsen, X. Carreo, J. S. Ashta, M. B. Knudsen, and G. F. Pedersen, "Probe selection in multi-probe OTA setups," *IEEE Trans. Antennas Propag.*, vol. 62, no. 4, pp. 2109–2120, Apr. 2014.
[31] H. Wang, W. Wang, Y. Wu, B. Tang, W. Zhang, and Y. Liu, "Probe selection for 5G massive MIMO base station over-the-air testing," *IEEE Antennas Wireless Propag. Lett.*, vol. 19, no. 11, pp. 1998–2002, Nov. 2020.
[32] W. Fan, I. Szini, J. Ø. Nielsen, and G. F. Pedersen, "Channel spatial correlation reconstruction in flexible multi-probe setups," *IEEE Antennas Wireless Propag. Lett.*, vol. 12, pp. 1724–1727, Jan. 2014.
[33] H. Wang, W. Wang, H. Gao, Y. Wu, Y. Liu, and J. Gao, "Plane wave compensation technique for multiple-input multiple-output over-the-air testing in small multi-probe anechoic chamber," *IET Microw., Antennas Propag.*, vol. 13, no. 15, pp. 2625–2631, Dec. 2019.
[34] D. He, B. Ai, K. Guan, L. Wang, Z. Zhong, and T. Kürner, "The design and applications of high-performance ray-tracing simulation platform for 5G and beyond wireless communications: A tutorial," *IEEE Commun. Surveys. Tutorials.*, vol. 21, no. 1, pp. 10–27, 1st Quart. 2019.
[35] H. Gao, W. Wang, Y. Wu, Y. Liu, and G. F. Pedersen, "A virtual over-the-air method for 5G massive MIMO base station testing with flexible virtual probes," *IEEE Access*, vol. 7, pp. 108474–108485, Jul. 2019.
[36] X. Gao, L. Dai, S. Han, C.-L. I, and R. W. Heath, Jr., "Energy-efficient hybrid analog and digital precoding for mmWave MIMO systems with large antenna arrays," *IEEE J. Sel. Areas Commun.*, vol. 34, no. 4, pp. 998–1009, Apr. 2016.
[37] F. Zhang, W. Fan, and Z. Wang, "Achieving wireless cable testing of high-order MIMO devices with a novel closed-form calibration method," *IEEE Trans. Antennas Propag.*, vol. 69, no. 1, pp. 478-487, 2021.
[38] R. Zhang, K. Xiong, Y. Lu, B. Gao, P. Fan and K. B. Letaief, "Joint Coordinated Beamforming and Power Splitting Ratio Optimization in MU-MISO SWIPT-Enabled HetNets: A Multi-Agent DDQN-Based Approach," *IEEE J. Sel. Areas Commun.*, vol. 40, no. 2, pp. 677-693, Feb. 2022.
[39] Y. Zhang, Z. Yuan, L. Tian, and J. Zhang, "A novel random angular sampling method for spatial and temporal channel emulation," *IEEE Wireless Commun. Lett.*, vol. 8, no. 5, pp. 1381–1385, Oct. 2019.
[40] W. Wang, H. Wang, Y. Wu and Y. Liu, "Novel Deterministic Angular Sampling Methods for 3D Channel Models," *IEEE Commun. Lett.*, vol. 25, no. 6, pp. 1756-1760, Jun. 2021.
[41] Y. Ji, W. Fan, G. F. Pedersen, and X. Wu, "On channel emulation methods in multiprobe anechoic chamber setups for over-the-air testing," *IEEE Trans. Veh. Technol.*, vol. 67, no. 8, pp. 6740–6751, Aug. 2018.
[42] P. Stoica and R. L. Moses, *Spectral analysis of signals*. Pearson/Prentice Hall Upper Saddle River, NJ, 2005.
[43] TR 38.901, "Study on channel model for frequencies from 0.5 to 100 GHz," 3GPP, Tech. Rep. V14.1.1, Jul. 2017.
[44] W. Fan, X. Carreno Bautista de Lisbona, F. Sun, J. Ø. Nielsen, M. B. Knudsen, and G. F. Pedersen, "Emulating spatial characteristics of MIMO channels for OTA testing," *IEEE Trans. Antennas Propag.*, vol. 61, no. 8, pp. 4306–4314, Aug. 2013.
[45] S. Boyd and L. Vandenberghe, *Convex Optimization*. Cambridge, U.K.: Cambridge Univ. Press, 2004.
[46] G. Zhang, K. Saito, W. Fan, X. Cai, P. Hanpinitsak, J.-I. Takada, and G. F. Pedersen, "Experimental characterization of millimeter-wave indoor propagation channels at 28 GHz," *IEEE Access*, vol. 6, pp. 76516–76526, Nov. 2018.
[47] S. S. Zhekov, O. Franek, and G. F. Pedersen, "Dielectric properties of common building materials for ultrawideband propagation studies," *IEEE Antennas Propag. Mag.*, vol. 62, no. 1, pp. 72–81, Feb. 2020.
[48] G. Zhang, J. Ø. Nielsen, X. Cai, K. Saito, P. Hanpinitsak, J. I. Takada, G. F. Pedersen, and W. Fan, "Modeling Multi-Frequency Characteristics for Classroom and Hall Scenarios at 2-4, 9-11 and 27-29 GHz Bands," *IEEE Access*, vol. 9, pp. 14549-14563, Jan. 2021.
[49] X. Cai and W. Fan, "A complexity-effificient high resolution propagation parameter estimation algorithm for ultra-wideband large-scale uniform circular array," *IEEE Trans. Commun.*, vol. 67, no. 8, pp. 5862–5874, Aug. 2019.